JCI The Journal of Clinical Investigation

Human muscle–derived stem/progenitor cells promote functional murine peripheral nerve regeneration

Mitra Lavasani, Seth D. Thompson, Jonathan B. Pollett, Arvydas Usas, Aiping Lu, Donna B. Stolz, Katherine A. Clark, Bin Sun, Bruno Péault, Johnny Huard

Research Article

Peripheral nerve injuries and neuropathies lead to profound functional deficits. Here, we have demonstrated that muscle-derived stem/progenitor cells (MDSPCs) isolated from adult human skeletal muscle (hMDSPCs) can adopt neuronal and glial phenotypes in vitro and ameliorate a critical-sized sciatic nerve injury and its associated defects in a murine model. Transplanted hMDSPCs surrounded the axonal growth cone, while hMDSPCs infiltrating the regenerating nerve differentiated into myelinating Schwann cells. Engraftment of hMDSPCs into the area of the damaged nerve promoted axonal regeneration, which led to functional recovery as measured by sustained gait improvement. Furthermore, no adverse effects were observed in these animals up to 18 months after transplantation. Following hMDSPC therapy, gastrocnemius muscles from mice exhibited substantially less muscle atrophy, an increase in muscle mass after denervation, and reorganization of motor endplates at the postsynaptic sites compared with those from PBS-treated mice. Evaluation of nerve defects in animals transplanted with vehicle-only or myoblast-like cells did not reveal histological or functional recovery. These data demonstrate the efficacy of hMDSPC-based therapy for peripheral nerve injury and suggest that hMDSPC transplantation has potential to be translated for use in human neuropathies.

Find the latest version:

https://jci.me/44071/pdf

Human muscle–derived stem/progenitor cells promote functional murine peripheral nerve regeneration

Mitra Lavasani,[1,2,3] Seth D. Thompson,[1,2] Jonathan B. Pollett,[1,2,4] Arvydas Usas,[1,2] Aiping Lu,[1,2] Donna B. Stolz,[5] Katherine A. Clark,[5] Bin Sun,[1,6] Bruno Péault,[1,6,7] and Johnny Huard[1,2,3,8]

[1]Stem Cell Research Center, [2]Department of Orthopaedic Surgery, and [3]Department of Bioengineering, University of Pittsburgh, Pittsburgh, Pennsylvania, USA. [4]Allegheny-Singer Research Institute, Pittsburgh, Pennsylvania, USA. [5]Department of Cell Biology and Physiology and [6]Department of Pediatrics, University of Pittsburgh, Pittsburgh, Pennsylvania, USA. [7]UCLA Orthopaedic Hospital Research Center, UCLA, Los Angeles, California, USA. [8]Department of Molecular Genetics and Biochemistry, University of Pittsburgh, Pittsburgh, Pennsylvania, USA.

Peripheral nerve injuries and neuropathies lead to profound functional deficits. Here, we have demonstrated that muscle-derived stem/progenitor cells (MDSPCs) isolated from adult human skeletal muscle (hMDSPCs) can adopt neuronal and glial phenotypes in vitro and ameliorate a critical-sized sciatic nerve injury and its associated defects in a murine model. Transplanted hMDSPCs surrounded the axonal growth cone, while hMDSPCs infiltrating the regenerating nerve differentiated into myelinating Schwann cells. Engraftment of hMDSPCs into the area of the damaged nerve promoted axonal regeneration, which led to functional recovery as measured by sustained gait improvement. Furthermore, no adverse effects were observed in these animals up to 18 months after transplantation. Following hMDSPC therapy, gastrocnemius muscles from mice exhibited substantially less muscle atrophy, an increase in muscle mass after denervation, and reorganization of motor endplates at the postsynaptic sites compared with those from PBS-treated mice. Evaluation of nerve defects in animals transplanted with vehicle-only or myoblast-like cells did not reveal histological or functional recovery. These data demonstrate the efficacy of hMDSPC-based therapy for peripheral nerve injury and suggest that hMDSPC transplantation has potential to be translated for use in human neuropathies.

Introduction

Despite recent advances in microsurgical techniques and improved understanding of nerve regeneration, functional recovery following repair of transected peripheral nerves often remains disappointing (1, 2). Loss of nerve and muscle function, impaired sensation, and painful neuropathies remain the major challenges (3). Therefore, there has been growing enthusiasm for the use of stem cell–based therapies for peripheral nerve regeneration (4–8). This concept is based on the ability of transplanted stem/progenitor cells to survive, engraft, and promote the recovery process by cell differentiation into tissue-specific cell types, signaling through cell-to-cell contact, or sustained release of neurotrophic factors. These properties may be the basis of an early regenerative stage that leads to increased target organ reinnervation through less axonal dieback.

Adult stem cells capable of adopting the neural and/or glial phenotypes in vitro can be isolated from murine or human CNS (9–11), bone marrow (12–15), umbilical cord blood (16–18), skin (19), hair follicles (20–22), adipose tissue (23–29), or dental pulp (30, 31). Stem/progenitor cells isolated from murine and human skeletal muscles by various methods give rise to progeny cells with neuronal and glial phenotypes (12, 32–36). Populations of slowly adhering cells isolated from skeletal muscle via the modified preplate technique called muscle-derived stem/progenitor cells (MDSPCs) (37–39) are characterized by sustained self-renewal, long-term proliferation, and multipotent differentiation capacities (37, 40, 41). MDSPCs can engraft and stimulate the regen-

eration of skeletal and cardiac muscles, bone, articular cartilage, and replenish the bone marrow of lethally irradiated mice (37, 40, 42–46). Their high therapeutic value is likely due to their superior survival capability under conditions of oxidative and hypoxic stresses and high expression of antioxidants relative to more differentiated cells, such as myoblasts (47, 48). Most recently, our findings showed that i.p. transplantation of young MDSPCs into progeroid mice leads to tissue regeneration in multiple organ systems and stimulates host tissue neovascularization (49), supporting a potential therapeutic value in numerous age-related diseases.

Prior studies in our laboratory examined the effects that various growth factors, such as BMP4, nerve growth factor (NGF), and VEGF, have on the fate of MDSPCs (37, 40, 42, 50). BMP4 promotes osteogenesis (40), while NGF and VEGF induce neurogenic and endothelial differentiation of MDSPCs, respectively (37, 40). In addition, NGF stimulation of MDSPCs significantly improves their engraftment efficiency in the *mdx* murine model of muscular dystrophy (50), suggesting a link between neurogenesis and myogenesis and substantiating the role of the environment in stem cell differentiation.

Our recent data suggest that MDSPCs, which can be isolated from human skeletal muscles (hMDSPCs) using the same technique (39), are likely mesenchymal stem cells of muscle origin and have the ability to undergo multilineage differentiation (51). In the present study, we examine the fate of hMDSPCs in controlled culture conditions and their potential for functional nerve repair. Our results indicate that hMDSPCs have the capacity to gain neuronal and glial phenotypes and provide evidence of their therapeutic capability in eliciting functional recovery and alleviating the skeletal muscle atrophy associated with nerve injury.
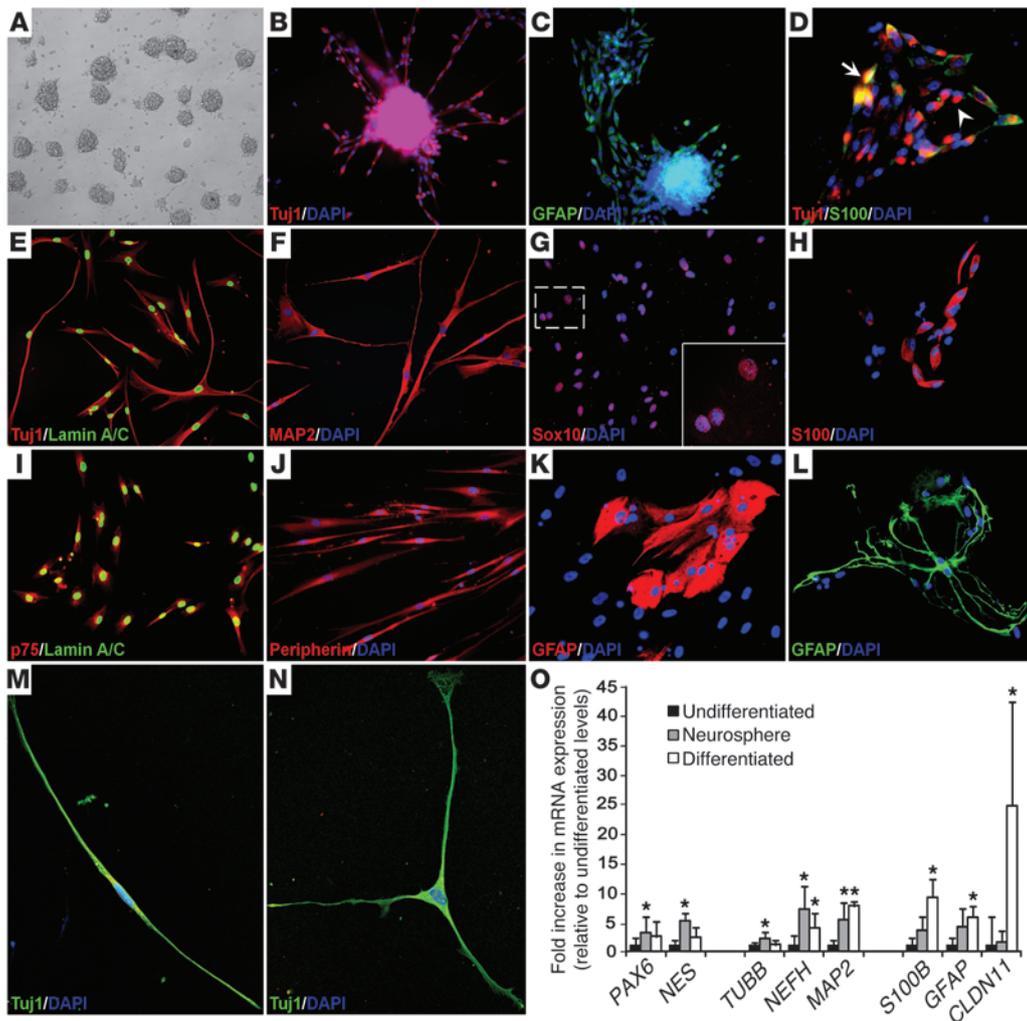
Figure 1
hMDSPCs adopt morphology and express markers of neuronal and glial cells under controlled culture conditions. Shown are representative images from at least six independent experiments from four hMDSPC populations (**A**) Bright-field image of hMDSPC-derived neurospheres 2 days after induction. Seven- to 8-day-old hMDSPC-derived neurospheres immunostained for (**B**) neuronal marker Tuj1 and (**C**) astrocytic and Schwann cell marker GFAP. (**D**) Dissociated 7- to 8-day-old neurospheres stained for Tuj1 (red) and S100 (green). Arrowhead shows cells Tuj1+ (red), and arrow indicates coexpression of Tuj1 and S100 (yellow). Terminally differentiated neurospheres at 14 to 27 days contain neurons expressing (**E**) Tuj1 and (**F**) MAP2 and cells expressing glial and Schwann cell markers (**G**) SOX10, (**H**) S100, (**I**) p75, (**J**) peripherin, (**K**) GFAP+ astrocyte type 1, and (**L**) GFAP+ astrocyte type 2. Tuj1+ cells show (**J**) bipolar and (**K**) tripolar neurons. The nuclear counterstain is DAPI (blue) or human lamin A/C (green). (**O**) Real-time RT-PCR was performed to measure expression levels of neural progenitor cell markers (*PAX6* and *NES*), neuronal markers (*TUBB*, *NEFH*, and *MAP2*), and glial and Schwann cell markers (*S100B*, *GFAP*, and *CLDN11*) between undifferentiated hMDSPCs, hMDSPC-derived neurospheres, and terminally differentiated hMDSPCs. Error bars indicate the mean ± SD from three independent hMDSPC populations; *$P < 0.05$, Tukey's test. Original magnification, ×20 (**A–C**, **E–G**, **I**, **J**, and **L**) and ×40 (**D**, **H**, **K**, **M**, **N**, and inset in **G**).

Results

hMDSPCs differentiate into phenotypically mature neuronal and glial cells under controlled culture conditions. Two days after culture in NeuroCult proliferation medium (Figure 1A), hMDSPCs gave rise to neurospheres. hMDSPC-derived neurospheres expressed neural- and glial-specific proteins, such as the neuron-specific class III β-tubulin (Tuj1) (Figure 1B) and the astrocyte marker glial fibrillary acidic protein (GFAP) (Figure 1C). hMDSPC-derived neurospheres also contained cells that coexpressed Tuj1 (red) and Schwann cell protein S100 (green) (Figure 1D, arrow), while others only expressed Tuj1 (Figure 1D, arrowhead). Coexpression

of neuronal and glial cell markers in vitro has been previously reported in hippocampal stem cells treated with basic FGF (bFGF) in serum-free medium (52), embryonic striatum at early stages of differentiation (53), immortalized embryonic mesencephalic cells (54), and postnatal forebrain neural progenitors (55). Our findings indicate that, like multipotent CNS progenitor cells, hMDSPCs remain partially differentiated and lack commitment to a specific path of differentiation.

Dissociated hMDSPC-derived neurospheres (5–8 days) maintained in differentiation conditions for 14 to 27 days were then immunostained for multipotent differentiation analysis. These
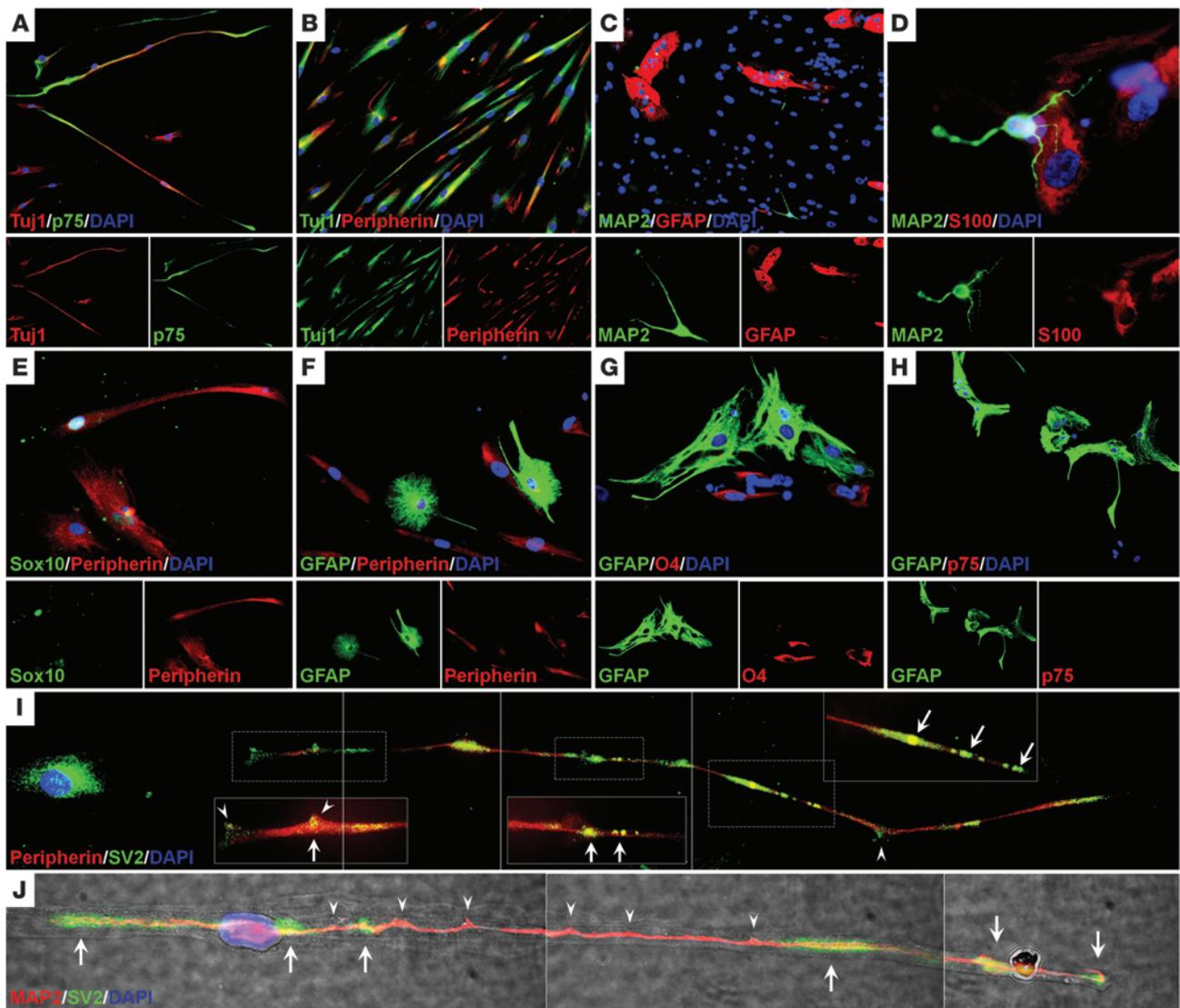
Figure 2
Terminally differentiated hMDSPCs show PNS and CNS phenotypes. hMDSPC-derived neurospheres (7–8 days old) were dissociated and maintained in differentiation medium for 21 to 27 days and immunostained for coexpression of (**A**) Tuj1 and p75, (**B**) Tuj1 and peripherin, (**C**) MAP2 and GFAP, (**D**) MAP2 and S100, (**E**) SOX10 and peripherin, (**F**) GFAP and peripherin, (**G**) GFAP and O4, and (**H**) GFAP and p75. (**I**) Composite image of a peripherin⁺ hMDSPC showing punctuate immunofluorescence expression of SV2, a synaptic vesicle protein marker, in the cell body and along the axonal shaft (arrows in higher-magnification boxed panels), including the protuberances (arrowheads). (**J**) Merged fluorescence and phase images of a MAP2⁺ hMDSPC expressing SV2 and shown as a composite. Data represent five independent experiments using four independent hMDSPC populations. Original magnification, ×20 (**A**–**C**, **E**–**G**), ×40 (**H**), ×60 (**D**, **I**, and **J**), and ×100 (inset in **I**).

terminally differentiated hMDSPCs generated Tuj1⁺ (Figure 1E) and MAP2⁺ (Figure 1F) neurons as well as glial and Schwann cells expressing SOX10 (Figure 1G), S100 (Figure 1H), p75⁺ (Figure 1I), peripherin (Figure 1J), and GFAP⁺ (Figure 1, K and L). Notably, hMDSPC-GFAP⁺ astrocytes showed a large, flat fibroblast-like morphology, known as type 1 astrocytes (Figure 1K), and smaller neuron-like cells with several branching processes (56), known as type 2 astrocytes (Figure 1L). Tuj1⁺ hMDSPCs also exhibited bipolar and tripolar morphologies (Figure 1, M and N, respectively).

Tuj1⁺ hMDSPC neurons coexpressed p75 (~14%, Figure 2A) and peripherin (~75%, Figure 2B). Cultures from terminally differentiated hMDSPCs contained mature neurons expressing MAP2 or glial/Schwann cells expressing GFAP (Figure 2C) or S100 (Figure 2D), but none of the cells coexpressed these neuronal and glial markers. Immunostaining for SRY box–containing gene 10 (SOX10), a nuclear transcription factor required for differentiation and maintenance of functional Schwann cells in the adult peripheral nervous system (PNS) (57), showed coexpression of this marker with peripherin in differentiated hMDSPCs (Figure 2E). We found that hMDSPCs expressing peripherin (Figure 2F) and the oligodendrocyte marker O4 (Figure 2G) were mutually exclusive from cells with astrocyte-like morphology expressing GFAP. GFAP⁺ cells displayed astrocytic rather than peripheral glial morphology and did not express p75 (Figure 2H). Moreover, we found
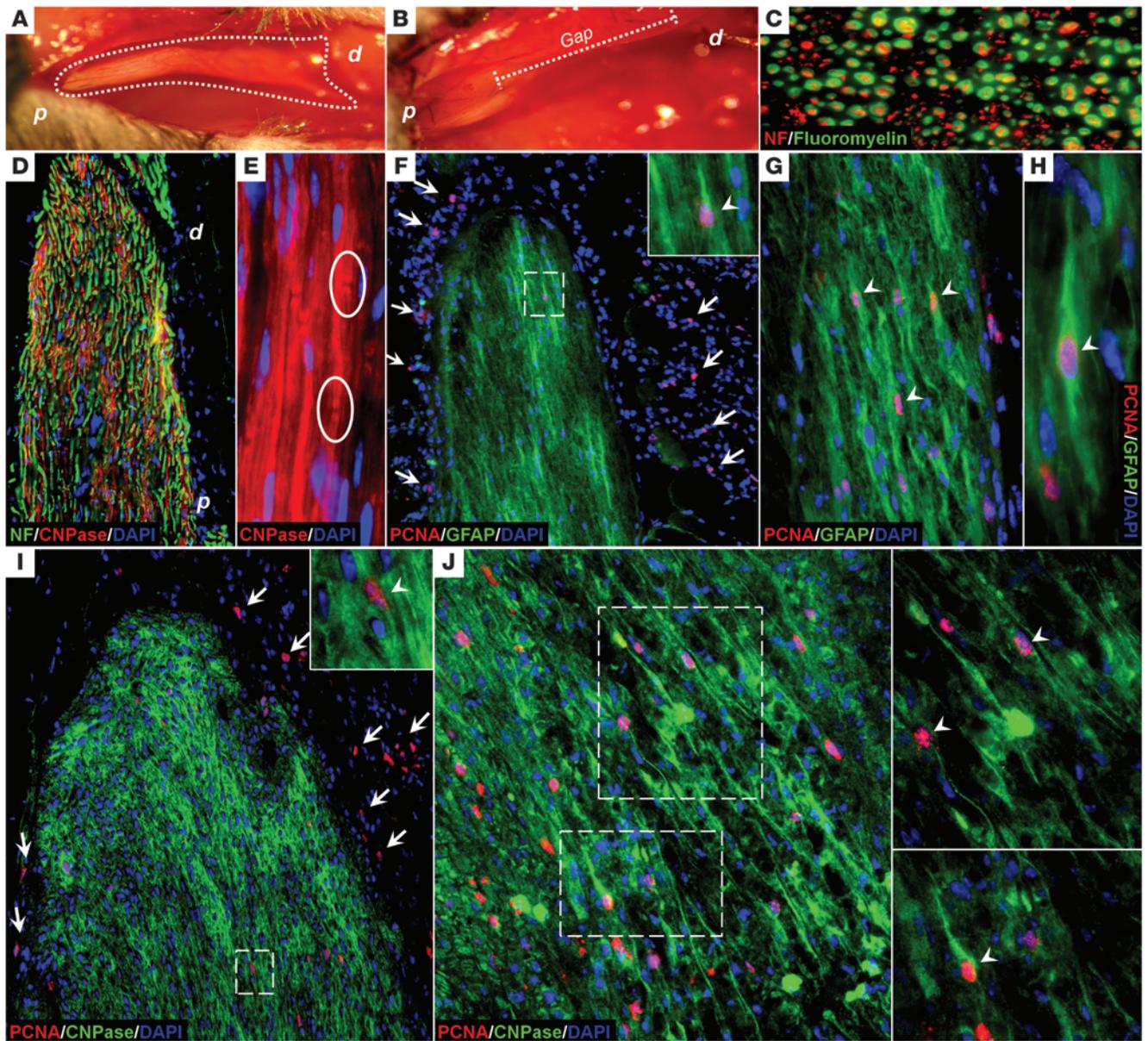
Figure 3

hMDSPCs survive, engraft, and promote peripheral nerve regeneration. (**A**) Representative image of complete nerve regeneration from proximal (*p*) to distal (*d*) stumps 6 weeks after injury and after hMDSPC transplantation into critical-sized sciatic nerve defects in SCID mice. (**B**) Minimal regeneration (Gap) in PBS-injected mice at 6 weeks. (**C**) Cross section of hMDSPC-regenerated nerve immunostained for NF and counterstained with FluoroMyelin. (**D**) Longitudinal sections of regenerating nerve immunostained for NF and CNPase. (**E**) CNPase staining of the regenerated nerve revealed nodes of Ranvier–like structures (white circles). (**F**) Human-specific PCNA+ donor cells surrounding (arrows) and infiltrating (inset, arrowhead) the growth cone of the regrowing nerve immunostained for GFAP 3 days after transplantation. (**G**) Representative image of colocalized human PCNA+ donor cells with Schwann cell marker GFAP within the regenerating nerve at 3 days. (**H**) Random representative image of colocalization at higher magnification. (**I**) Representative image showing engraftment (arrows) and integration (inset, arrowhead) of PCNA+ human donor cells at the proximal growth cone of the regenerating nerve immunostained with Schwann cell marker CNPase at 4 weeks. (**J**) Grafted hMDSPCs coexpressing PCNA and CNPase (arrowheads) at 5 days. Images in **I** and **J** insets show a higher magnification of the dashed boxes. Engraftment and colocalization were determined by screening more than 10,000 donor cells from 4 independent transplanted hMDSPC populations within 982 sections of 122 tissues obtained from 12 mice. The nuclear counterstain is DAPI (blue). Original magnification, ×10 (**I**), ×20 (**D**, **F**, and **J**), ×40 (**C** and **G**), ×60 (**E** and insets in **F**, **I**, and **J**), and ×100 (**H**).

Table 1
Primers for quantitative real-time RT-PCR

Gene name	Gene accession number	Primer sequence (5′–3′) (forward, reverse)	Amplicon position (start to end)
PAX6	NM_001604	CCGGCAGAAGATTGTAGAGCT, CCGTTGGACACGTTTTGATTG	510–630
NES	NM_006617	GACTTCCCTCAGCTTTCAGG, CCGTTGGACACGTTTTGATTG	1096–1179
TUBB	NM_178014	CTGGACCGCATCTCTGTGTA, AAAGGACCTGAGCGAACAGAG	257–370
NEFH	NM_021076	CAGGACCTGCTCAATGTCAAG, CCTTCTGGAAGCGAGAAAGGA	1189–1308
MAP2	NM_001039538	CCAATGGATTCCCATACAGGG, CTCTCCGTTGATCCCATTCTC	585–686
S100B	NM_006272	TATTCTGGAAGGGAGGGAGAC, CCACAACCTCCTGCTCTTTGA	163–275
GFAP	NM_002055	CTGGAGGTTGAGAGGGACAAT, CAGCCTCAGGTTGGTTTCATC	423–504
CLDN11	NM_005602	CTGGTGTTTTGCTCATTCTGC, AGCCTGCATACAGGGAGTAG	558–675

that the presynaptic vesicle marker synaptic vesicle protein 2 (SV2) was distributed in a punctuate pattern, with prominent localization in the cell body and throughout the axon shafts, including the protuberances (arrowheads) of peripherin+ (Figure 2I, arrows) and MAP2+ (Figure 2J, arrows) neurons.

Immunofluorescence staining of undifferentiated hMDSPCs, hMDSPC-derived neurospheres, and differentiated hMDSPCs for two PNS marker proteins, peripherin and p75, revealed that 29% of undifferentiated hMDSPCs expressed peripherin and 23% of cells were positive for p75. These values increased at the stage of neurosphere formation to 45% and 43%, respectively. At the terminal differentiation stage, peripherin expression significantly increased to 65% (*$P < 0.05$ relative to undifferentiated hMDSPCs and hMDSPC-derived neurospheres, Tukey's test) while the expression level of p75 was significantly reduced to 13% (*$P < 0.05$ relative to neurospheres, Tukey's test). We also carried out real-time RT-PCR analysis using three independent hMDSPC populations to obtain expression profiles of specific neuronal and glial cell genes (Table 1) before and after differentiation (Figure 1O). The differentiation of hMDSPCs into neurospheres increased the expression of the neuroectodermal markers PAX6 and NES, genes expressed in neural stem cells and neurospheres (3-fold and 5-fold, respectively; *$P < 0.05$, Tukey's test). Expression of the neuronal cell markers TUBB, NEFH, and MAP2 increased in the neurospheres (2-fold, 7-fold and 5-fold, respectively). After terminal differentiation, expression of the neuronal marker TUBB decreased to the same level as that observed in undifferentiated cells, however, expression levels of mature neuronal markers NF and MAP2 increased (4-fold and 8-fold, respectively) compared with levels in undifferentiated hMDSPCs (*$P < 0.05$, Tukey's test). The astroglial and/or Schwann cell markers S100B and GFAP were also upregulated at the terminal differentiation stage (10-fold and 5-fold, respectively) when compared with those in the undifferentiated control cells (*$P < 0.05$, Tukey's test). Furthermore, the terminal differentiation of hMDSPCs revealed a 25-fold upregulation (*$P < 0.05$, Tukey's

test) in the expression of the oligodendrocyte-specific marker CLDN11. Together, these results demonstrate that hMDSPCs have the potential to differentiate into neuronal cells and glial cells, including myelin-producing Schwann cells.

hMDSPCs promote histological regeneration of critical-sized sciatic nerve defects after injury. hMDSPCs from four separate donors were transplanted into critical-sized sciatic nerve defects in SCID mice ($n = 96$ mice, 4 hMDSPC populations). Complete sciatic nerve regeneration from the proximal (*p*) to distal (*d*) stumps was visually observed as early as 6 weeks after injury in the hMDSPC-transplanted groups (Figure 3A), whereas the presence of nerve gaps in the PBS-injected group ($n = 20$ mice) exhibited minimal regeneration (Figure 3B) at the same time after injury. As with the PBS-injected animals, mice transplanted with myoblast-like cells did not show significant regeneration ($n = 18$ mice, 3 populations) (Supplemental Figure 1; supplemental material available online with this article; doi:10.1172/JCI44071DS1). Of note, blood vessel networks were also present around all regenerated nerves. Cross sections of regenerated nerves exhibited NF+ axons (red) enclosed by FluoroMyelin+ cells (Figure 3C, green). Longitudinal sections of regenerating nerves exhibited both NF (green) and 2′,3′-cyclic-nucleotide 3′-phosphodiesterase (CNPase, red) immunoreactivity (Figure 3D). Furthermore, CNPase+ myelinated axons (red) of the regenerated sciatic nerve revealed node of Ranvier–like structures (Figure 3E, white circles), identified by the short nerve segments that had no CNPase immunoreactivity. From 3 days to 18 weeks after injury and hMDSPC transplantation ($n = 25$ mice), human proliferating cell nuclear antigen–positive (PCNA-positive) cells were surrounding the growth cone of the regenerating nerve (arrows in Figure 3F, at 6 weeks and in Figure 3I at 4 weeks). Some of the donor cells (PCNA+, red) integrated into the myelinated regenerating nerve and exhibited expression of the Schwann cell markers GFAP (green, inset in Figure 3F and arrowheads in Figure 3, G and H) and CNPase (green, inset Figure 3I, arrowheads in Figure 3J). In addition, donor-derived Schwann cells expressing PCNA (blue) in CNPase+ myelin sheets (green) surrounded NF+ axons (red) and were detected in the middle and distal regions of the regenerated nerve (Figure 4, A and B, respectively). These data demonstrate that hMDSPCs are able to differentiate into myelin-producing Schwann cells in a PNS environment in vivo.

We also assessed the site of hMDSPC engraftment for inflammation by immunofluorescence staining for the myeloid cell and granulocyte marker Gr-1 in conjunction with CNPase and PCNA. On days 1 through 7 after transplantation, numerous infiltrating Gr-1+ cells were detected at the site of injury (Supplemental Figures 2–5). The number of Gr-1+ cells was reduced noticeably starting on days 16 and 21 (Supplemental Figures 6 and 7), and cells were rarely detectable at 28 days (Supplemental Figure 8). In addition, hMDSPC-transplanted mice also showed no sign of tumor formation at the site of injury up to 18 months after transplantation ($n = 20$ mice, 4 hMDSPC populations).

To investigate the survival and engraftment of myoblast-like cells, which are incapable of regenerating the nerve defect, we examined tissues 16 days ($n = 3$) and 4 weeks ($n = 3$) after injury and hMDSPC transplantation to determine cell survival. Sections
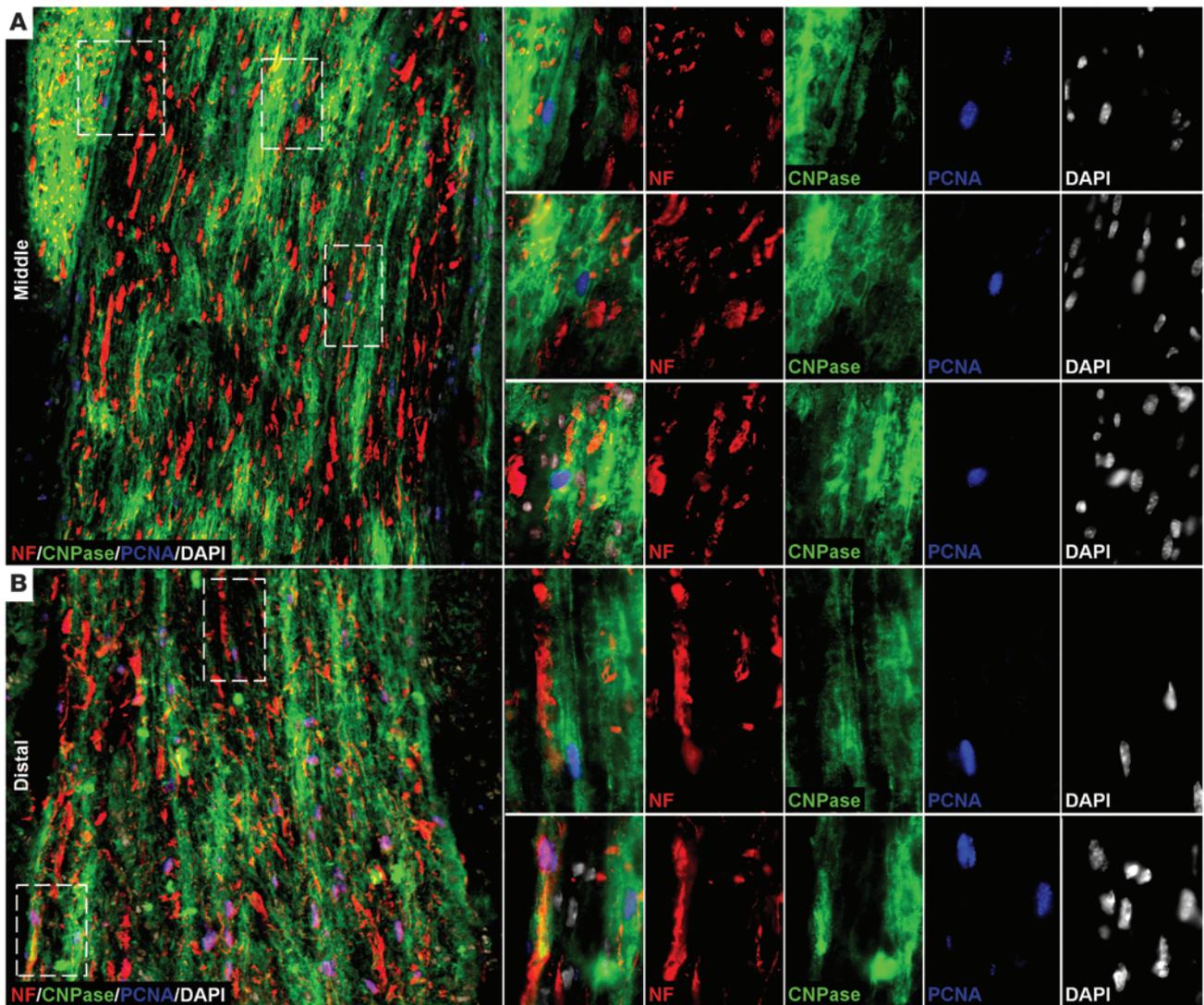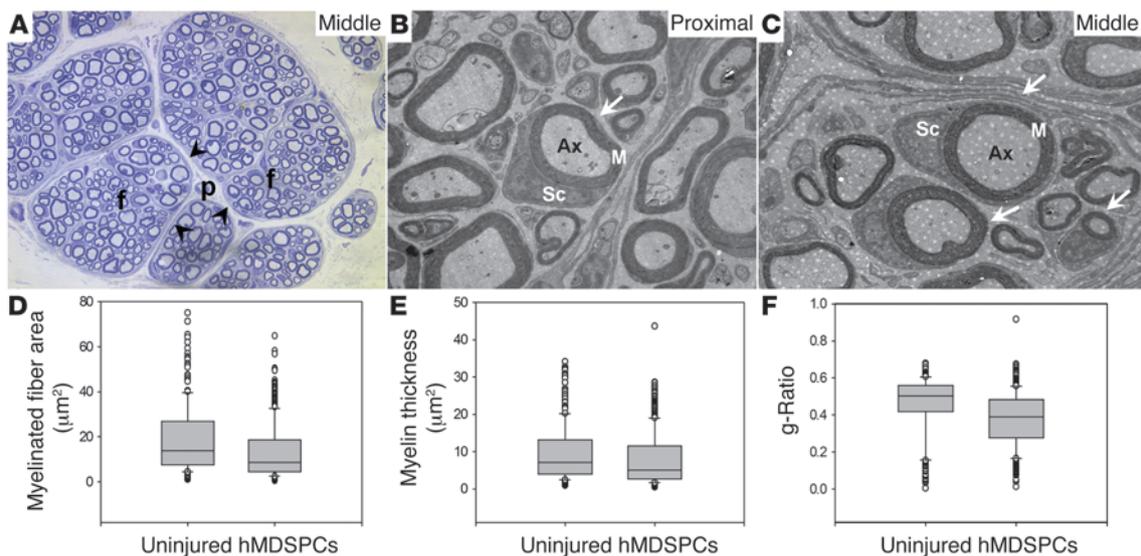
Figure 4
hMDSPCs integrate into the microenvironment of the regenerated nerve and generate myelinating Schwann cells. Representative images are of immunostained longitudinal sections of hind limbs, including the regenerating sciatic nerve, 4 weeks after injury and after hMDSPC transplantation. Low- and high-magnification images show immunostaining for neurons (NF, red), myelinating Schwann cells (CNPase, green), human donor cell nuclei (PCNA, blue), and DAPI (white) to identify all nuclei. Donor PCNA+ hMDSPCs were detected inside the regenerated nerve in immediate proximity to the myelinated axons and expressed NF and CNPase at the middle (**A**) and distal (**B**) regions of the regenerating nerve. Panels on the right show higher-magnification images of the chosen area (dashed boxes), highlighting the colocalization. Engraftment and colocalization were determined by screening more than 10,000 donor cells from 4 independent transplanted hMDSPC populations within 982 sections of 122 tissues obtained from 12 mice. Original magnification, ×20 (**A** and **B**) and ×100 (dashed boxes).

were immunostained for PCNA and NF and at 16 days detected PCNA+ donor myoblasts surrounding and integrating into the growth cone of the regenerating axons positive for NF (arrows, Supplemental Figure 1A). Although we still detected PCNA+ donor myoblasts 4 weeks after transplantation, the NF+ axons showed a great degree of degeneration (Supplemental Figure 1B) versus regenerating nerve in hMDSPC-transplanted mice (Figure 4).

hMDSPCs promote functional recovery of critical-sized sciatic nerve defects after injury. Furthermore, 12 weeks after transplantation of hMDSPCs, the regenerated nerves contained many nerve fibers with organized fascicles (f) surrounded by perineurium (p, arrows) (Figure 5A). The mid-sections of the regenerated sciatic nerves

contained an average of 450 ± 21 myelinated axons compared with 356 ± 17 in uninjured control nerves, showing a statistically significant difference ($P = 0.002$, 1-way ANOVA). Pairwise multiple comparisons showed a significant difference ($P < 0.05$, Tukey's test) between axons in uninjured control and hMDSPC-transplanted groups, while we observed no significant difference between the hMDSPCs isolated from different donors. Transmission electron microscopy at proximal and mid-sections of the regenerated nerves revealed proper histological regeneration, many myelinated Schwann cells (arrows), and the absence of connective tissue fibrosis (Figure 5, B and C, respectively). The myelinated axons in the hMDSPC group showed a median cross-sectional area of $8.6 \ \mu m^2$

Figure 5
hMDSPCs promote nerve fiber regeneration and remyelination. (**A**) Sections from regenerated nerve 12 weeks after transplantation stained with toluidine blue. Arrowheads indicated the perineurium (p) surrounding the nerve fascicles (f). (**B** and **C**) Transmission electron microscopy of proximal and mid-sections, respectively, of the regenerated nerves at 12 weeks; Sc, Schwann cells; M, myelin sheath; Ax, axon. (**D**–**F**) Quantification of the morphometric parameters at mid-sections of the regenerated nerve from the hMDSPC transplanted group and the uninjured control group at 12 weeks (>1,500 fibers from the hMDSPC group, $n = 3$ mice from three independent populations; >600 fibers from the uninjured group, $n = 3$ mice, respectively) were analyzed for (**D**) myelinated fiber area, (**E**) myelin thickness, and (**F**) g-ratios (axonal area/myelinated fiber area). Horizontal bar indicates the median (50th percentile). Box represents the 25th–75th percentiles, and error bars represent the 10th–90th percentiles. Original magnification, ×10 (**A**) and ×800 (**B** and **C**).

versus 15.5 μm² for uninjured control nerves (Figure 5D; $P < 0.001$, Mann-Whitney rank sum test) and a median myelin thickness of 5.2 μm² versus 8.1 μm² (Figure 5E; $P < 0.001$, Mann-Whitney rank sum test). The median and 25th–75th percentiles of the g-ratios (axonal area/myelinated fiber area) in mid-sections of the regenerated nerves were 0.48 and 0.41–0.54, respectively, as compared with 0.49 and 0.4–0.58 for the uninjured control group (Figure 5F; $P = 0.063$). This difference was not statistically significant, indicating a close resemblance between the hMDSPC-regenerated nerves and uninjured nerves.

We examined functional recovery by holding the mice vertically by their tails with their forelimbs slightly touching the floor. Twelve weeks after injury, hMDSPC-transplanted mice presented qualitative improvement in their ability to hold their injured hind leg (right leg) at the same level as the contralateral uninjured leg (normal, left leg), while mice with the nerve gap treated with PBS showed common signs of abnormal posture. hMDSPC-transplanted mice also displayed wider qualitative toe spreading compared with that of the PBS-treated group (Supplemental Video 1).

Quantitative paw print analyses obtained from walking tracks revealed functional recovery of hMDSPC-transplanted mice at 2, 4, 8, 12, and 14 weeks (Figure 6A, $n = 96$ mice at 2 weeks, $n = 96$ mice at 4 weeks, $n = 72$ mice at 8 weeks, $n = 72$ mice at 12 weeks, and $n = 48$ mice at 14 weeks) in comparison with myoblast- or PBS-treated mice (Figure 6B, $n = 18$ and $n = 20$ mice per treatment group, respectively). This improvement in hMDSPC-transplanted mice was also supported by significant functional recovery of the toe spread (TS) factor, print length (PL) factor, and sciatic functional index (SFI) compared with myoblast- and PBS-treated mice at all time points tested after injury, except for hMDSPCs isolated from donor 4, which did

not show significant functional recovery of the PL factor compared with the myoblast-treated group at 2 weeks. These differences started by week 2 and became highly evident by 14 weeks, at which point the average TS factor of the hMDSPC-transplanted groups showed significant recovery (0.193 ± 0.03) versus the myoblast- (0.431 ± 0.07; §$P < 0.05$, Tukey's test) and PBS-treated mice (0.514 ± 0.02; *$P < 0.05$, Tukey's test). The average PL factor was also significantly improved (0.157 ± 0.02) compared with that of the myoblast- (0.301 ± 0.03; §$P < 0.05$, Dunn's test) and PBS-treated mice (0.338 ± 0.05; *$P < 0.05$, Dunn's test). The TS and PL recovery led to significant improvement in the average SFI of hMDSPC-transplanted mice (-35.2 ± 2.9) versus that of myoblast-transplanted mice (-78.6 ± 7.6; §$P < 0.05$, Tukey's test) and PBS-treated mice (-86.1 ± 6.8; *$P < 0.05$, Tukey's test). These results provide evidence of reproducibility between the preplate hMDSPC populations and their consistent beneficial effect on peripheral nerve regeneration and functional recovery after injury.

hMDSPCs reverse muscle atrophy. Since muscle atrophy and a decline in neuromuscular innervation are known to be important endogenous causes of sarcopenia, we measured the gastrocnemius muscle weights to assess muscle atrophy and analyzed AChR distribution to investigate the reorganization of the motor endplates. We observed loss of muscle mass in both the hMDSPC- and PBS-treated groups at 5, 10, and 15 weeks (Figure 7A). Five weeks after injury, the average weight of the hMDSPC- and PBS-treated gastrocnemius muscles (0.05 ± 0.015 g and 0.05 ± 0.012 g, respectively) was decreased when compared with that of the uninjured control groups (0.11 ± 0.008 g; *$P < 0.05$, Tukey's test). While the PBS-treated group continued to show progressive loss of muscle mass 20 weeks after
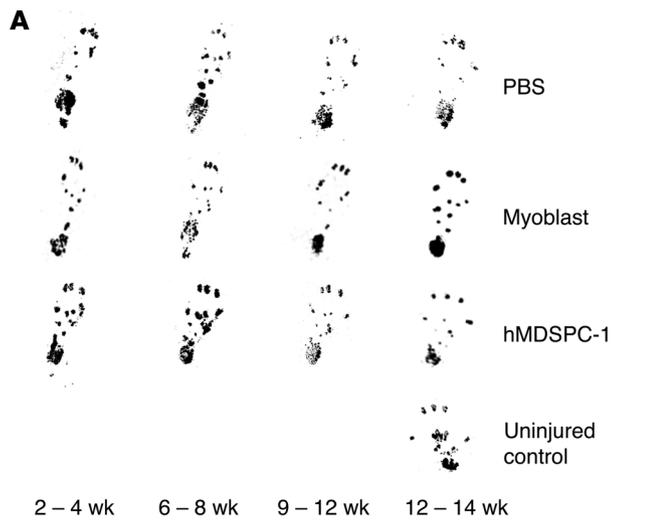
Figure 6

hMDSPC transplantation improves functional recovery after sciatic nerve transection. Assessment of the functional recovery of regenerated sciatic nerve was performed using a walking track assessment. (**A**) Representative paw print patterns from mice transplanted with PBS, myoblasts, or hMDSPCs shown in consecutive weeks after implantation. Quantification of paw prints for (**B**) TS factor, (**C**) PL factor, and (**D**) SFI in hMDSPC-transplanted versus myoblast- and PBS-treated mice at consecutive weeks after denervation. Error bars indicate the mean ± SD. Plotted are average analyses of paw prints (4–5 paired paw prints/mouse) collected from PBS- ($n = 20$), myoblast- ($n = 18$), and hMDSPC-treated groups ($n = 96$ mice at 2 weeks, $n = 96$ mice at 4 weeks, $n = 72$ mice at 8 weeks, $n = 72$ mice at 12 weeks, and $n = 48$ mice at 14 weeks). *$P < 0.05$, comparing the individual hMDSPC populations isolated from individual donors 1–4 with PBS (Dunn's test or Tukey's test) or the three averaged populations of myoblasts ($^§P < 0.05$, Dunn's test). Comparison of PL factor from hMDSPCs isolated from donor 4 with that of the myoblast group at 2 weeks was not significant (NS, Dunn's test).
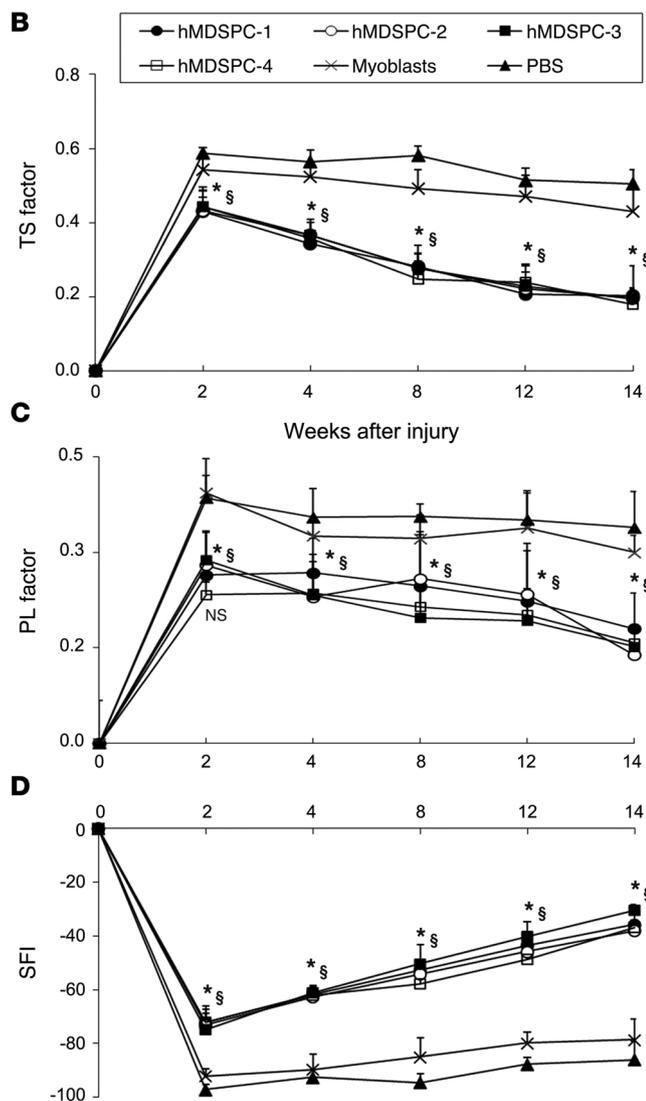
injury compared with the uninjured control (0.03 ± 0.001 g; *$P < 0.05$, Tukey's test), the hMDSPC-transplanted mice began to display signs of recovery (0.07 ± 0.005 g; *$P < 0.05$, Tukey's test). We observed no recovery in the PBS-treated mice, as they displayed a constant decline of muscle mass out to 72 weeks (0.02 ± 0.002, Tukey's test). Remarkably, 72 weeks after injury, the gastrocnemius muscles of the hMDSPC-transplanted mice exhibited no significant difference in weight (0.09 ± 0.009 g; Dunn's test) when compared with that of their contralateral uninjured control muscles (0.10 ± 0.007 g), indicating proper reinnervation of the target skeletal muscle tissues.

In order to determine whether the decrease in muscle mass was the result of actual myofiber atrophy, cross sections of the gastrocnemius muscles from each group were stained for dystrophin (Figure 7B), and fiber cross-sectional areas were measured and compared between groups. The host myofiber area distribution showed that most of the individual dystrophin+ fibers in the hMDSPC-transplanted group and uninjured control group had fiber areas greater than 2,000 μm², whereas most of the fibers in the PBS-treated group had areas between 0 and 400 μm², with an increased amount of interstitial connective tissue (Figure 7C). This indicates that the transplantation of hMD-SPCs into the nerve defect could restore the cross-sectional areas of the denervated muscle fibers to near-complete histological recovery.

To assess the significance of alterations to the neuromuscular junctions (NMJs), we examined the level of postsynaptic endplates in the gastrocnemius muscles. Confocal z-stack images of postsynaptic AChR clusters labeled with α-bungarotoxin (α-BTX, green) revealed mature motor endplates in both the uninjured control and the post-72-week hMDSPC-transplanted groups (Figure 8A). Gastrocnemius muscles of hMDSPC-transplanted mice showed reorganization of motor endplates, with endplate perforations at the postsynaptic sites following reinnervation. We observed that the motor endplates in the PBS-treated groups were substantially altered, showing dispersed and extensive fragmentation, which led to the elimination of proper endplate distribution and complete degeneration (Figure 8A). Indeed, α-BTX staining could not be detected in some of the PBS-treated muscles, indicating a total loss of postsynaptic AChR clusters (data not shown). The average ratio of α-BTX+ AChRs (green) to dystrophin+ myofibers (red) was analyzed to determine the effect that denervation had on the number of AChRs present in the gastrocnemius muscles (Figure 8B). The hMDSPC-transplanted mice had
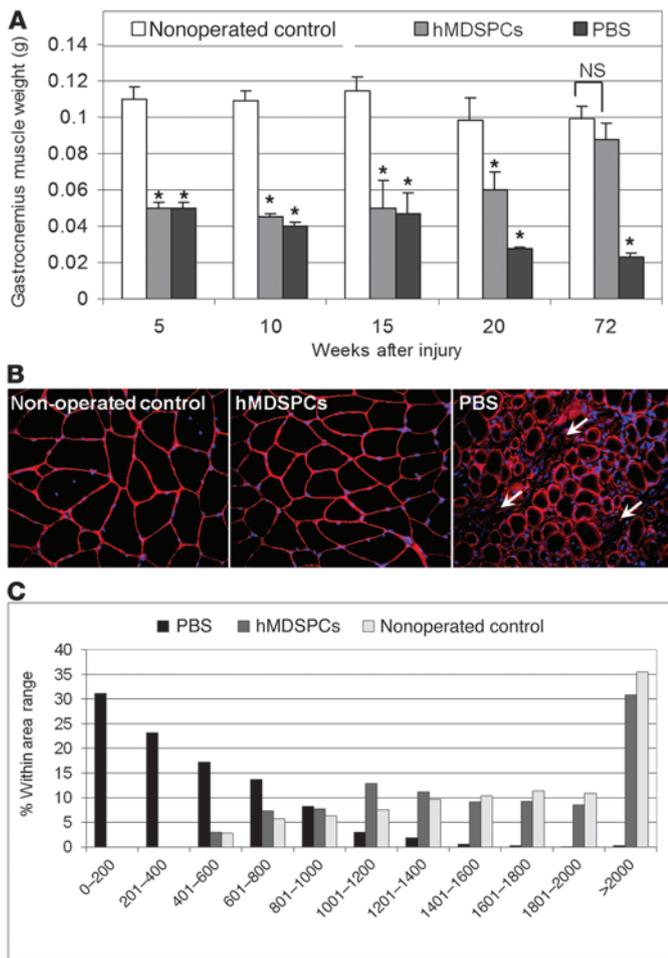
Figure 7
hMDSPC transplantation reduces muscle atrophy associated with sciatic nerve injury. (**A**) Plotted are the average gastrocnemius muscle weights of uninjured control, hMDSPC- and PBS-treated mice calculated from 4 to 6 mice at each time point ± SD (*$P < 0.05$, Tukey's test; NS, not significant.) (**B**) Representative images of gastrocnemius muscle sections stained for dystrophin (red) to identify the host myofiber areas. Arrows indicate the area of interstitial connective tissue. Original magnification, ×40. (**C**) Histogram of the cross-sectional area distribution of host myofibers in the PBS-treated (black bars) and hMDSPC-treated (dark gray bars) groups compared with those in uninjured control group (light gray bars). Plotted is the average number of myofibers of each size range calculated from more than 3,500 fibers in 4 to 8 sections analyzed per mouse ($n = 5$); the hMDSPC group is averaged from three independent hMDSPC populations. Distribution of fiber size is indicated on the x axis, representing increasingly more mature fibers with increased size.

a ratio (23% ± 6.8%) that was at a near-normal level when compared with that of the uninjured control group (25% ± 6.3%) 72 weeks after transplantation (Figure 8C). The gastrocnemius muscles of the PBS-treated mice showed an extensive reduction in the density of postsynaptic AChR clusters (1.5% ± 0.9%, $P < 0.05$, Dunn's test), further confirming marked alterations in postdenervation NMJs.

Discussion

Here, we aimed to investigate the fate of hMDSPCs, stem/progenitor cells isolated from adult human skeletal muscle, using

well-established techniques in culture and a PNS injury model. Our in vitro results demonstrate that hMDSPCs express neuronal and glial phenotypes, preferentially Schwann cells, under controlled culture conditions (Figures 1 and 2).

In our in vivo studies, the implantation of hMDSPCs into a critical-sized sciatic nerve defect in mice restored nerve function via nerve fiber regeneration through myelin-producing Schwann cells. The presence of human-specific PCNA^{+} donor cells at the growth cone of the proximal nerve stump through the regeneration process (Figures 3) indicates that these cells survive and surround the regenerating axons to promote myelination and axonal growth (Figure 5). We observed that some hMDSPCs also infiltrated the regenerating nerve and differentiated into myelin-producing Schwann cells ensheathing closely associated axons (Figure 4). Although there was substantial donor cell engraftment, given their low number in relation to host cells, the sole mechanism for the observed significant histological and functional regeneration was not likely due to donor cell differentiation. Previous evidence suggests that MDSPCs exert their regenerative function at least in part via secreting factors that promote changes in host cell activities (49). These observations support the concept that hMDSPCs may confer their therapeutic effect through the release of stimulatory factor(s) to induce endogenous axonal growth through chemoattraction of myelinating Schwann cells that are most likely host derived. Schwann cells are known to release various neurotrophic substances that are key regulatory proteins in the modulation of neuronal survival, axonal elongation, synaptic plasticity, and neurotransmission (58). Therefore, mechanisms that may contribute to the nerve healing observed here include the recruitment of host cells to the site of injury, proliferation, and differentiation of host cells toward a supporting cell lineage, such as Schwann cells, which release cytokines that exert neuroprotective effects independently of neurogenesis (59, 60). Thus, our results suggest that the observed regeneration is, at least in part, mediated via a paracrine/endocrine mechanism(s), as previously discussed (61, 62). In fact, our recent results demonstrate that young functional MDSPCs can restore the dysfunction of aged MDSPCs when cocultured and, when transplanted, are able to rescue the homeostasis of mice with accelerated aging through secreted factors that act systemically (49), suggesting that cultures' exogenous and lesions' endogenous factors likely determine the fate of donor stem cells.

The chronic axotomy of motor neurons and chronic denervation fully accounts for poor functional recovery, degradation of AChRs in NMJs (63), and irreversible muscle atrophy (64). However, Sulaiman and Gordon (65) showed that chronically denervated muscle fibers tend to survive and accept reinnervation; therefore, prompt motor axon reinnervation of muscle results in faster functional recovery. In the current study, we demonstrate that mice transplanted with hMDSPCs displayed efficient motor nerve terminal reinnervation of skeletal muscle, leading to reversal of muscle atrophy (Figure 7). Reorganization of NMJs in the muscle (Figure 8) and attenuation of muscle atrophy led to an increase in muscle mass and myofiber size after cell transplantation, promoting functional gait recovery (Figure 6). In addition, the severity of muscle atrophy is directly related to the length of time required for the regenerating axons to reach the denervated muscle (66). Interestingly, Salpeter and colleagues (67) found that the degrada-
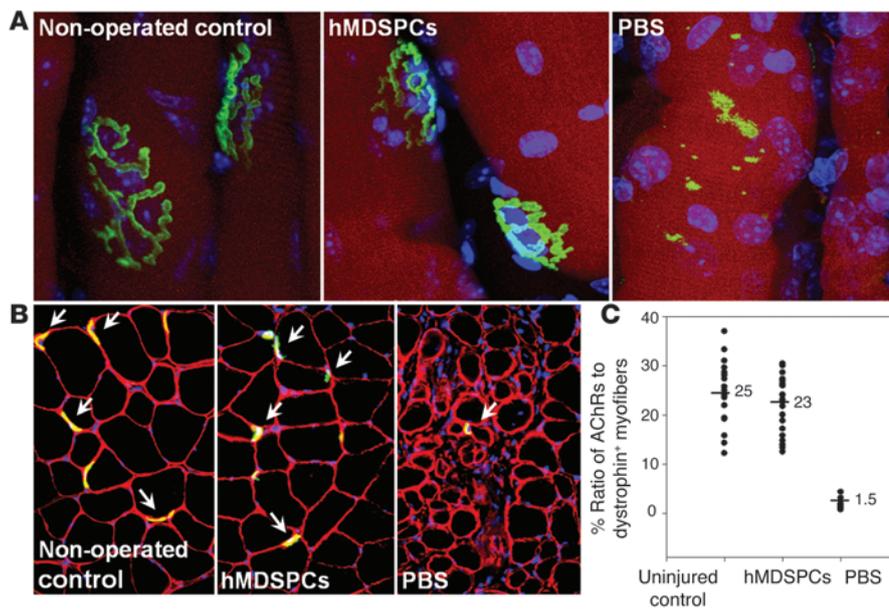
Figure 8
hMDSPC transplantation promotes muscle reinnervation after injury. (**A**) Confocal images of whole-mount gastrocnemius muscles of uninjured controls compared with those of hMDSPC- and PBS-treated mice 72 weeks after transplantation. The f-actin in muscle fibers was labeled with phalloidin (red), the postsynaptic AChRs with α-BTX (green), and the cell nuclei with DAPI (blue). (**B**) Representative sections from gastrocnemius muscles ($n = 6$) immunostained with dystrophin (red), α-BTX (green), and DAPI (blue) 72 weeks after transplantation. (**C**) Plotted is the ratio of AChRs/host dystrophin+ myofibers in hMDSPC- and PBS-treated groups relative to the contralateral uninjured control myofibers ($n = 4$–5 mice per group). Horizontal bar represents the median. Original magnification, ×60 (**A**) and ×40 (**B**).

tion rate of the original junctional receptors is highly dependent on the continued presence of the nerve; hence, the reinnervation slowed the degradation rate and reversed the effect of denervation on the original AChRs. These observations may explain why muscle atrophy is found to be reduced in our cell transplanted groups, because these groups show continuous progressive axonal regeneration and greater muscle reinnervation.

Of note, although the B6 SCID mice lack lymphocytes and hence an adaptive immune response, the integrity of their innate immunity is preserved (68) and is capable of eliminating human donor cells (69). Except for an anticipated acute inflammatory response at the lesion site during the first week, we did not detect granulocyte or myeloid cell infiltration at later time points (Supplemental Figures 2–8). The evidence that human donor cells are detected weeks after the acute inflammatory response is delineated and that the transected nerve is functionally regenerated supports the proposal for hMDSPCs as an effective cell therapy. Previous findings have indicated that, similar to other stem cells (70, 71), MDSPCs display immune-privileged properties (37), including their ability to survive, divide, and participate in wound healing in a similar fashion in normal and SCID mice (72). Moreover, even though tumor formation is common after neuronal axotomy (73), we observed no sign of tumor formation at the site of injury up to 18 months after transplantation. In addition, a reduction in fibrosis and an increase in neovascularization could be other key factors explaining the faster recovery we observed in the hMDSPC group, since it would enable endogenous progenitor cells to penetrate the defect area and establish early and effective reinnervation. Since it is essential to retain the cells at the site of nerve injury, future studies will aim to use hMDSPCs in combination with implantable conduits and injectable hydrogels, such as those with controlled release of growth factor(s) (74), which we believe could further enhance the rate of axonal growth and blood vessel formation and lead to improved recovery.

Taken together, this study demonstrates that human skeletal muscle is a rich and promising source of stem/progenitor cells for the treatment of demyelinating disorders. The therapeutic potential of hMDSPCs provides promise for future clinical applications to achieve functional recovery after injury or peripheral neuropathies and to prevent muscle atrophy.

Methods

Cell isolation and culturing. hMDSPCs were isolated from four human skeletal muscle biopsies (mean age 23 years; range, 18–30 years) via the preplate technique previously described (37, 38, 40). The rapidly adhering cells (pp1–pp5) and slowly adhering cells (pp6) were isolated based on their characteristics of adhesion to collagen type 1–coated culture flasks. The cells were maintained in proliferation medium containing DMEM (Invitrogen) with 10% horse serum (Invitrogen), 10% FBS (Invitrogen), 1% penicillin-streptomycin (Invitrogen), and 0.5% chick embryo extract (Accurate Chemical and Scientific Corporation).

Neurosphere formation and differentiation. Neurosphere formation and differentiation were performed using the instructions provided by STEM-CELL Technologies with appropriate modifications described in detail in the Supplemental Methods.

Immunocytochemistry. All immunocytochemistry protocols are detailed in the Supplemental Methods.

Real-time RT-PCR. Real-time RT-PCR was performed on RNA from four independent hMDSPC populations using the cDNA and primer sequences listed in Table 1. Procedural details are described in the Supplemental Methods.

Cell transplantation. The sciatic nerves of 6- to 8-week-old SCID mice (B6.CB17-*Prkdc^scid^*/SzJ; The Jackson Laboratory) were exposed, and a 4- to 5-mm segment of the nerve was removed, resulting in a ~6.5- to 7-mm defect due to retraction of the nerve endings. Immediately thereafter, animals were implanted with a viable single-cell suspension of 4×10^5 hMDSPCs (slowly adhering, pp6), myoblast-like cells (rapidly adhering, pp3), or an equal volume (15 μl) of PBS (vehicle, control) at the site of the proximal and distal nerve stumps, and the wound was sutured closed. We randomly selected mice from each group to sacrifice at designated time points for each study after transplantation, and the hind limbs, including the sciatic nerves, were harvested, flash-frozen in 2-methylbutane precooled in liquid nitrogen, serially sectioned at 6-μm thickness, and stored at –80°C for further analysis.

Immunohistochemistry. All immunohistochemistry protocols are detailed in the Supplemental Methods.

Inflammatory response. To evaluate the degree of inflammation around the engraftment site after injury and after hMDSPC transplantation, longitudinal cryosections of hind limbs, including the sciatic nerves, were immunostained for Ly6G and Ly6C (Gr-1), a marker for myeloid cells and granulocytes, as described in detail in the Supplemental Methods.

Morphometric analysis of the regenerated nerve. The degree of myelination was evaluated using light and transmission electron microscopy according to detailed protocols described in the Supplemental Methods.

Muscle reinnervation. The gastrocnemius muscles of injured (transplanted with hMDSPCs or PBS) and contralateral uninjured control legs were isolated, and the wet weights were recorded. Collected data were normalized to the values of the uninjured control legs for each mouse and reported. Quantitation of myofiber area distribution and postsynaptic AChR receptor densities are described in detail in the Supplemental Methods.

Functional assessment. Quantitative functional recovery was evaluated by measuring paw tracks obtained from mice walking in a 6 × 46 cm corridor (straight maze) lined with white paper (Benchkote; Cardinal Health) and featuring an opening at one end to a darkened compartment. The hind paws of the animals were pressed onto the surface of a black waterproof ink pad, and the animals' feet were immediately washed in lukewarm water at the end of the tests. Mice were randomly selected from the uninjured controls, PBS-, myoblast-, and hMDSPC-implanted groups for analysis. After two or three conditioning trials, the animals were walked to obtain measurable footprints. The collected paw prints were scanned with a Microtek 9800XL scanner. Measurements were collected from the footprints in a blinded fashion using Northern Eclipse software to obtain two different parameters: the distance between the first and fifth toes, known as TS, and the distance from the heel to the distal end of the third toe, known as PL. TS factors, PL factors, and SFI for each time point were calculated using the formulas derived by Inserra et al. (75). Factors were obtained using the values from a normal (uninjured, left leg) footprint and the contralateral experimental (injured, right leg) footprint for each mouse. The factor measurements were calculated by averaging values from 4 to 5 footprints. An SFI of 0 reflects normal function, and an SFI of –100 indicates total loss of function.

Statistics. All Statistical analyses were carried out using the SigmaStat software package, version 2.0 (Jandel Scientific). We used a 2-tailed Student's t test or the Mann-Whitney rank sum test (where appropriate) for direct comparisons between treatment and control groups. For multiple comparisons, the 1-way ANOVA or the Kruskal-Wallis 1-way ANOVA on ranks (where appropriate) was applied. Pairwise multiple comparisons were performed using the Dunn's test or Tukey's test following rank-based ANOVA. All values are expressed as the mean ± SD. A P value of less than 0.05 was considered statistically significant.

Study approval. Experiments involving mice were reviewed and approved by the IACUC of the University of Pittsburgh (Animal Welfare Assurance Number A3187-01) under approved protocol 0810153A-2 (formerly protocol 13-03) and were in accordance with NIH guidelines for the humane care of animals. Human skeletal muscle biopsies were obtained from the National Disease Research Interchange (NDRI) under the University of Pittsburgh IRB 0305079 entitled "Isolation of Human Muscle-derived Stem Cells." Patients' written informed consent was received by the NDRI.

Address correspondence to: Johnny Huard or Mitra Lavasani, Department of Orthopaedic Surgery, University of Pittsburgh, School of Medicine, Stem Cell Research Center, Bridgeside Point II, 450 Technology Drive, Suite 206, Pittsburgh, Pennsylvania 15219, USA. Phone: 412.648.2798; Fax: 412.648.4066; E-mail: jhuard@pitt.edu (J. Huard). Phone: 412.624.5626; Fax: 412.648.4066; E-mail: mil39@pitt.edu (M. Lavasani).

1. Millesi H. Progress in peripheral nerve reconstruction. *World J Surg.* 1990;14(6):733–747.
2. Fu SY, Gordon T. The cellular and molecular basis of peripheral nerve regeneration. *Mol Neurobiol.* 1997; 14(1-2):67–116.
3. Evans GR. Challenges to nerve regeneration. *Semin Surg Oncol.* 2000;19(3):312–318.
4. Dezawa M, Takahashi I, Esaki M, Takano M, Sawada H. Sciatic nerve regeneration in rats induced by transplantation of in vitro differentiated bone-marrow stromal cells. *Eur J Neurosci.* 2001;14(11):1771–1776.
5. Tohill M, Mantovani C, Wiberg M, Terenghi G. Rat bone marrow mesenchymal stem cells express glial markers and stimulate nerve regeneration. *Neurosci Lett.* 2004;362(3):200–203.
6. Amoh Y, et al. Human hair follicle pluripotent stem (hfPS) cells promote regeneration of peripheral-nerve injury: an advantageous alternative to ES and iPS cells. *J Cell Biochem.* 2009; 107(5):1016–1020.
7. Walsh SK, Gordon T, Addas BM, Kemp SW, Midha R. Skin-derived precursor cells enhance peripheral nerve regeneration following chronic denervation. *Exp Neurol.* 2010;223(1):221–228.
8. Schaakxs D, Kalbermatten DF, Raffoul W, Wiberg M, Kingham PJ. Regenerative cell injection in denervated muscle reduces atrophy and enhances recovery following nerve repair. *Muscle Nerve.* 2013; 47(5):691–701.
9. Reynolds BA, Weiss S. Generation of neurons and astrocytes from isolated cells of the adult mammalian central nervous system. *Science.* 1992;255(5052):1707–1710.
10. Palmer TD, Ray J, Gage FH. FGF-2-responsive neuronal progenitors reside in proliferative and quiescent regions of the adult rodent brain. *Mol Cell Neurosci.* 1995;6(5):474–486.
11. Gritti A, et al. Multipotential stem cells from the adult mouse brain proliferate and self-renew in response to basic fibroblast growth factor. *J Neurosci.* 1996;16(3):1091–1100.
12. Romero-Ramos M, et al. Neuronal differentiation of stem cells isolated from adult muscle. *J Neurosci Res.* 2002;69(6):894–907.
13. Woodbury D, Schwarz EJ, Prockop DJ, Black IB. Adult rat and human bone marrow stromal cells differentiate into neurons. *J Neurosci Res.* 2000; 61(4):364–370.
14. Black IB, Woodbury D. Adult rat and human bone marrow stromal stem cells differentiate into neurons. *Blood Cells Mol Dis.* 2001;27(3):632–636.
15. Kabos P, Ehtesham M, Kabosova A, Black KL, Yu JS. Generation of neural progenitor cells from whole adult bone marrow. *Exp Neurol.* 2002; 178(2):288–293.
16. Sanchez-Ramos JR, et al. Expression of neural markers in human umbilical cord blood. *Exp Neurol.* 2001;171(1):109–115.
17. Buzanska L, Machaj EK, Zablocka B, Pojda Z, Domanska-Janik K. Human cord blood-derived cells attain neuronal and glial features in vitro. *J Cell Sci.* 2002;115(Pt 10):2131–2138.
18. Kogler G, et al. A new human somatic stem cell from placental cord blood with intrinsic pluripotent differentiation potential. *J Exp Med.* 2004; 200(2):123–135.
19. Toma JG, et al. Isolation of multipotent adult stem cells from the dermis of mammalian skin. *Nat Cell Biol.* 2001;3(9):778–784.
20. Amoh Y, et al. Implanted hair follicle stem cells form Schwann cells that support repair of severed

peripheral nerves. *Proc Natl Acad Sci U S A*. 2005; 102(49):17734–17738.
21. Hunt DP, et al. A highly enriched niche of precursor cells with neuronal and glial potential within the hair follicle dermal papilla of adult skin. *Stem Cells*. 2008;26(1):163–172.
22. Amoh Y, et al. Human and mouse hair follicles contain both multipotent and monopotent stem cells. *Cell Cycle*. 2009;8(1):176–177.
23. Safford KM, et al. Neurogenic differentiation of murine and human adipose-derived stromal cells. *Biochem Biophys Res Commun*. 2002;294(2):371–379.
24. Safford KM, Safford SD, Gimble JM, Shetty AK, Rice HE. Characterization of neuronal/glial differentiation of murine adipose-derived adult stromal cells. *Exp Neurol*. 2004;187(2):319–328.
25. Fujimura J, Ogawa R, Mizuno H, Fukunaga Y, Suzuki H. Neural differentiation of adipose-derived stem cells isolated from GFP transgenic mice. *Biochem Biophys Res Commun*. 2005;333(1):116–121.
26. Kingham PJ, et al. Adipose-derived stem cells differentiate into a Schwann cell phenotype and promote neurite outgrowth in vitro. *Exp Neurol*. 2007; 207(2):267–274.
27. Xu Y, et al. Neurospheres from rat adipose-derived stem cells could be induced into functional Schwann cell-like cells in vitro. *BMC Neurosci*. 2008;9:21.
28. Anghileri E, et al. Neuronal differentiation potential of human adipose-derived mesenchymal stem cells. *Stem Cells Dev*. 2008;17(5):909–916.
29. Jang S, Cho HH, Cho YB, Park JS, Jeong HS. Functional neural differentiation of human adipose tissue-derived stem cells using bFGF and forskolin. *BMC Cell Biol*. 2010;11:25.
30. Karbanová J, Soukup T, Suchánek J, Pytlík R, Corbeil D, Mokrý J. Characterization of dental pulp stem cells from impacted third molars cultured in low serum-containing medium. *Cells Tissues Organs*. 2011;193(6):344–365.
31. Kiraly M, et al. Simultaneous PKC and cAMP activation induces differentiation of human dental pulp stem cells into functionally active neurons. *Neurochem Int*. 2009;55(5):323–332.
32. Tamaki T, et al. Clonal multipotency of skeletal muscle-derived stem cells between mesodermal and ectodermal lineage. *Stem Cells*. 2007;25(9):2283–2290.
33. Vourc'h P, et al. Isolation and characterization of cells with neurogenic potential from adult skeletal muscle. *Biochem Biophys Res Commun*. 2004; 317(3):893–901.
34. Alessandri G, et al. Isolation and culture of human muscle-derived stem cells able to differentiate into myogenic and neurogenic cell lineages. *Lancet*. 2004;364(9448):1872–1883.
35. Schultz SS, Lucas PA. Human stem cells isolated from adult skeletal muscle differentiate into neural phenotypes. *J Neurosci Methods*. 2006; 152(1-2):144–155.
36. Arsic N, Mamaeva D, Lamb NJ, Fernandez A. Muscle-derived stem cells isolated as non-adherent population give rise to cardiac, skeletal muscle and neural lineages. *Exp Cell Res*. 2008;314(6):1266–1280.
37. Qu-Petersen Z, et al. Identification of a novel population of muscle stem cells in mice: potential for muscle regeneration. *J Cell Biol*. 2002;157(5):851–864.
38. Gharaibeh B, et al. Isolation of a slowly adhering cell fraction containing stem cells from murine skeletal muscle by the preplate technique. *Nat Protoc*. 2008;3(9):1501–1509.
39. Lavasani M, et al. Isolation of muscle-derived stem/progenitor cells based on adhesion characteristics to collagen-coated surfaces. *Methods Mol Biol*. 2013;976:53–65.
40. Lee JY, et al. Clonal isolation of muscle-derived cells capable of enhancing muscle regeneration and bone healing. *J Cell Biol*. 2000;150(5):1085–1100.
41. Deasy BM, et al. Long-term self-renewal of postnatal muscle-derived stem cells. *Mol Biol Cell*. 2005; 16(7):3323–3333.
42. Peng H, et al. Synergistic enhancement of bone formation and healing by stem cell-expressed VEGF and bone morphogenetic protein-4. *J Clin Invest*. 2002;110(6):751–759.
43. Oshima H, et al. Differential myocardial infarct repair with muscle stem cells compared to myoblasts. *Mol Ther*. 2005;12(6):1130–1141.
44. Payne TR, et al. Regeneration of dystrophin-expressing myocytes in the mdx heart by skeletal muscle stem cells. *Gene Ther*. 2005;12(16):1264–1274.
45. Kuroda R, et al. Cartilage repair using bone morphogenetic protein 4 and muscle-derived stem cells. *Arthritis Rheum*. 2006;54(2):433–442.
46. Cao B, et al. Muscle stem cells differentiate into haematopoietic lineages but retain myogenic potential. *Nat Cell Biol*. 2003;5(7):640–646.
47. Urish KL, et al. Antioxidant levels represent a major determinant in the regenerative capacity of muscle stem cells. *Mol Biol Cell*. 2009;20(1):509–520.
48. Vella JB, Thompson SD, Bucsek MJ, Song M, Huard J. Murine and human myogenic cells identified by elevated aldehyde dehydrogenase activity: implications for muscle regeneration and repair. *PLoS One*. 2011;6(12):e29226.
49. Lavasani M, et al. Muscle-derived stem/progenitor cell dysfunction limits healthspan and lifespan in a murine progeria model. *Nat Commun*. 2012;3:608.
50. Lavasani M, Lu A, Peng H, Cummins J, Huard J. Nerve growth factor improves the muscle regeneration capacity of muscle stem cells in dystrophic muscle. *Hum Gene Ther*. 2006;17(2):180–192.
51. Gao X, et al. BMP2 is superior to BMP4 for promoting human muscle-derived stem cell-mediated bone regeneration in a critical-sized calvarial defect model. *Cell Transplant*. 2013;22(12):2393–2408.
52. Gage FH, et al. Survival and differentiation of adult neuronal progenitor cells transplanted to the adult brain. *Proc Natl Acad Sci U S A*. 1995; 92(25):11879–11883.
53. Rosser AE, Tyers P, ter Borg M, Dunnett SB, Svendsen CN. Co-expression of MAP-2 and GFAP in cells developing from rat EGF responsive precursor cells. *Brain Res Dev Brain Res*. 1997;98(2):291–295.
54. Colucci-D'Amato GL, Tino A, Pernas-Alonso R, ffrench-Mullen JM, di Porzio U. Neuronal and glial properties coexist in a novel mouse CNS immortalized cell line. *Exp Cell Res*. 1999;252(2):383–391.
55. Feldman DH, Thinschmidt JS, Peel AL, Papke RL, Reier PJ. Differentiation of ionic currents in CNS progenitor cells: dependence upon substrate attachment and epidermal growth factor. *Exp Neurol*. 1996;140(2):206–217.
56. Raff MC, Abney ER, Cohen J, Lindsay R, Noble M. Two types of astrocytes in cultures of developing rat white matter: differences in morphology, surface gangliosides, and growth characteristics. *J Neurosci*. 1983;3(6):1289–1300.
57. Bremer M, et al. Sox10 is required for Schwann-cell homeostasis and myelin maintenance in the adult peripheral nerve. *Glia*. 2011;59(7):1022–1032.
58. Dezawa M. Central and peripheral nerve regeneration by transplantation of Schwann cells and transdifferentiated bone marrow stromal cells. *Anat Sci Int*. 2002;77(1):12–25.
59. Maiese K, Boniece I, DeMeo D, Wagner JA. Peptide growth factors protect against ischemia in culture by preventing nitric oxide toxicity. *J Neurosci*. 1993;13(7):3034–3040.
60. Nozaki K, Finklestein SP, Beal MF. Basic fibroblast growth factor protects against hypoxia-ischemia and NMDA neurotoxicity in neonatal rats. *J Cereb Blood Flow Metab*. 1993;13(2):221–228.
61. Gharaibeh B, Lavasani M, Cummins JH, Huard J. Terminal differentiation is not a major determinant for the success of stem cell therapy - cross-talk between muscle-derived stem cells and host cells. *Stem Cell Res Ther*. 2011;2(4):31.
62. Gharaibeh B, Deasy B, Lavasani M, Cummins JH, Li Y, Huard J. Musculoskeletal tissue injury and repair: role of stem cells, their differentiation, and paracrine effects. In: Hill JA and Olson EN, eds. *Muscle: Fundamental Biology and Mechanisms of Disease*. New York, New York, USA: Elsevier Academic Press; 2012:881–897.
63. Levitt TA, Loring RH, Salpeter MM. Neuronal control of acetylcholine receptor turnover rate at a vertebrate neuromuscular junction. *Science*. 1980;210(4469):550–551.
64. Fu SY, Gordon T. Contributing factors to poor functional recovery after delayed nerve repair: prolonged denervation. *J Neurosci*. 1995;15(5 Pt 2):3886–3895.
65. Sulaiman OA, Gordon T. Effects of short- and long-term Schwann cell denervation on peripheral nerve regeneration, myelination, and size. *Glia*. 2000;32(3):234–246.
66. Kobayashi J, et al. The effect of duration of muscle denervation on functional recovery in the rat model. *Muscle Nerve*. 1997;20(7):858–866.
67. Salpeter MM, Cooper DL, Levitt-Gilmour T. Degradation rates of acetylcholine receptors can be modified in the postjunctional plasma membrane of the vertebrate neuromuscular junction. *J Cell Biol*. 1986;103(4):1399–1403.
68. Dorshkind K, et al. Functional status of cells from lymphoid and myeloid tissues in mice with severe combined immunodeficiency disease. *J Immunol*. 1984;132(4):1804–1808.
69. Shibata S, et al. Peritoneal macrophages play an important role in eliminating human cells from severe combined immunodeficient mice transplanted with human peripheral blood lymphocytes. *Immunology*. 1998;93(4):524–532.
70. Menendez P, Bueno C, Wang L, Bhatia M. Human embryonic stem cells: potential tool for achieving immunotolerance? *Stem Cell Rev*. 2005;1(2):151–158.
71. Yang XF. Immunology of stem cells and cancer stem cells. *Cell Mol Immunol*. 2007;4(3):161–171.
72. Radfar AJ, et al. Transplantation of virally transduced cells into the dermis of immunocompetent and immunodeficient (SCID) mice to determine gene expression profile and differential donor cell survival. *Wound Repair Regen*. 2000;8(6):503–510.
73. Lewin-Kowalik J, Marcol W, Kotulska K, Mandera M, Klimczak A. Prevention and management of painful neuroma. *Neurol Med Chir (Tokyo)*. 2006; 46(2):62–67.
74. Chu H, Gao J, Chen CW, Huard J, Wang Y. Injectable fibroblast growth factor-2 coacervate for persistent angiogenesis. *Proc Natl Acad Sci U S A*. 2011; 108(33):13444–13449.
75. Inserra MM, Bloch DA, Terris DJ. Functional indices for sciatic, peroneal, and posterior tibial nerve lesions in the mouse. *Microsurgery*. 1998;18(2):119–124.